Pergamon

*Acta mater.* Vol. 45, No. 11, pp. 4695–4702, 1997

Printed in Great Britain
PII: S1359-6454(97)00123-7
1359-6454/97 $17.00 + 0.00

# TOUGHNESS VARIATION OF FERROELECTRICS BY POLARIZATION SWITCH UNDER NON-UNIFORM ELECTRIC FIELD

**TING ZHU and WEI YANG†**

Department of Engineering Mechanics, Tsinghua University, Beijing 100084, China

*(Received 23 October 1996; accepted 11 March 1997)*

**Abstract**—Low fracture toughness of ferroelectric ceramics calls for a reliability concern in the development of smart structures. For ferroelectrics under mechanical and electrical loadings, the intensified stress and electric fields in the vicinity of a crack-like flaw lead to domain reorientation. The switched domains induce incompatible strain near the flaw and consequently change the apparent fracture toughness. The present paper investigates toughness variation by small scale polarization switching under non-uniform electric and stress fields. A two-term near tip electric field is obtained by analyzing a permeable elliptical flaw in a ferroelectric solid. Analytical solution for the shielding stress intensity factor is derived for the ideal situation of mono-domain ferroelectrics. The result is generated by a Reuss-type assembly to the poly-domain ferroelectrics. The predictions based on the present model explain the conflicting experimental data on the toughness variations with respect to the applied electric field. © *1997 Acta Metallurgica Inc.*

## 1. INTRODUCTION

Advances in modern technology set the ferroelectric ceramics at the center stage in the development of sensors and actuators in smart structures. However, ferroelectric ceramics are brittle and susceptible to cracking, raising the need for investigation of their toughening mechanisms. Experimental and theoretical analyses [1–7] indicated that domain switching plays an important role in the toughness variation of ferroelectrics. Under mechanical and electrical loadings, the intensified stress and electric fields in the vicinity of a crack-like flaw lead to domain reorientation. The switched domains induce incompatible strain under the constraint of unswitched material, and consequently alter the stress distribution near the flaw. The apparent toughness of ferroelectrics thus varies due to domain switching. In the experimental studies, Mehta and Virkar [2] examined domain switching by X-ray diffraction. Lynch *et al.* [3] observed residual switching by use of birefringence. Theoretically, switching induced toughness variation can be pursued in the same vein as transformation toughening in ceramics, see McMeeking and Evans [8], Budiansky *et al.* [9]. Taking into account the stress induced domain switching, Pisarenko *et al.* [1] and Mehta and Virkar [2] studied fracture toughness anisotropy for ferroelectrics under pure mechanical loading. Recently, Yang and Zhu [7] proposed a model to investigate stress activated switching caused by uniform electric field for ferroelectrics under combined mechanical and electrical loadings.

Whether the electric field impedes or enhances crack propagation is still a debatable issue. Several research groups [3, 10–13] reported conflicting experimental results. Park and Sun [10] performed compact tension tests and found that apparent fracture toughness varied asymmetrically for poled ferroelectrics under positive and negative electric fields. A positive field along the poling axis reduced the fracture load, while a negative one increased it. Tobin and Pak [11] and Lynch [4] reached the similar conclusions by using Vicker's indentation. On the other hand, Singh and Wang [12] observed an opposite trend. Namely the crack propagates less under a positive applied field, and longer under a negative one. Park and Sun [10] verified their experimental results by a criterion based on mechanical strain energy release rate. On the other hand, considering piezoelectric effect, Kumar and Singh [13] performed finite element analyses and their results checked with the experimental data of Singh and Wang [12]. To predict accurately the electric field influence, the nonlinear effect of domain reorientation near the crack tip is important, as pointed out by Suo [5]. Considering domain switching mechanism, Yang and Zhu [7] studied the toughening effect under uniform electric field, and their prediction is consistent with the observation of Park and Sun [10]. Nevertheless, the electric field in reality is non-uniform in the vicinity of the flaw. It is that non-uniform electric field distribution that may influence the toughness variation.

†To whom all correspondence should be addressed.

In this paper, a theoretical model for switching induced toughness variation is presented, which works for the situation of simultaneously applied stress and electric fields. We consider the case that both the stress and the electric fields are non-uniform. The model explores in detail the effect of non-uniform electric field on the mechanical fracture process. The plan of the paper is as follows. In the next section the non-uniform fields outside the switching zone are derived under the assumption of small scale domain switching. We adopt the criterion of polarization switch proposed by Hwang *et al.* [14] for an individual domain, in which domains switch when the combined (electric and mechanical) work reaches a threshold value. In Section 3 we evaluate toughness variation for mono-domain ferroelectrics. The analytical solution given there reveals several dimensionless material parameter groups of the problem. In Section 4, we propose a Reuss type poly-domain assembly to estimate the toughness variation of fully poled ferroelectrics.

## 2. SMALL SCALE DOMAIN SWITCHING

Attention is focused on the case of small scale switching, in the sense that the specimen size is considerably larger than the switching zone size. The merit of the small scale switching model can be appreciated as follows. Firstly, geometric complexities are separated from the domain switching process. More importantly, switching strain cannot be relieved by global deformation in the case of small scale switching, and thus contributes to toughen the ceramics.

### 2.1. *Non-uniform electric and stress fields*

We now derive the non-uniform fields outside the switching zone. As the first model to address this issue, we try to simplify the problem while retaining the key dimensionless material groups. Two assumptions are introduced: (1) the interaction between stress and electric fields is weak outside the switching zone; and (2) the material is modeled as elastically and dielectrically isotropic. Therefore, the non-uniform fields outside the switching zone can be determined by isotropic linear elasticity and electrostatics, respectively. The detailed structure of the coupled nonlinear fields near the flaw tip, as well as the slight anisotropy in material properties, are neglected.

We first evaluate non-uniform electric field. One controversial issue is the boundary conditions along the crack surface. Impermeable condition has been frequently adopted. However, results given by McMeeking [15] on electrostrictive solids and by Dunn [16] on piezoelectrics indicated that impermeable assumption may misinterpret the effects of the electric field on crack propagation. In reality, the small, but finite, crack volume contains air or some other gas whose dielectric constant does not vanish. Electric field may penetrate through the crack volume. We derive the electric field based on the solution for an elliptic flaw given by McMeeking [15]. As shown in Fig. 1, an electric field of strength $E^\infty$ is imposed perpendicular to the flaw. The permittivities of the elliptic flaw and the matrix are $\epsilon_f$ and $\epsilon_m$, respectively. Symbols $a$ and $b$ measure the lengths of the semi-axes of the ellipse. For the case of vertically applied remote electric field, the electric field outside the flaw can be obtained from equation (9) in [15]. After some rearrangement, it becomes

$$-E_1 + iE_2 = IE^\infty \frac{\zeta^2 + \dfrac{1-\kappa}{1+\kappa}}{\zeta^2 - \dfrac{1-\dfrac{b}{a}}{1+\dfrac{b}{a}}}, \tag{1}$$

where $E_1$ and $E_2$ are the components of the electric field in the $x$ and $y$ direction, and

$$z = x + iy = \frac{1}{2}[(a+b)\zeta + (a-b)\zeta^{-1}], \tag{2}$$

$$\kappa = \frac{a\epsilon_f}{b\epsilon_m}, \tag{3}$$

and $i = \sqrt{-1}$. The dimensionless parameter $\kappa$ represents the relative permeability of the flaw, encompassing both the flaw geometry and the dielectric parameters. The value of $\kappa$ is determined by the relative magnitude of the permittivities ratio $\epsilon_f/\epsilon_m$ and the aspect ratio $b/a$. Consider the case of $b \ll a$ but $1/\kappa$ is not necessarily small, equation (1) reduces to

$$-E_1 + iE_2 = iE^\infty \frac{\dfrac{1}{a^2}[z + \sqrt{z^2 - a^2}]^2 + \dfrac{1-\kappa}{1+\kappa}}{\dfrac{1}{a^2}[z + \sqrt{z^2 - a^2}]^2 - 1} \tag{4}$$

where appropriate branch has been selected. Taking

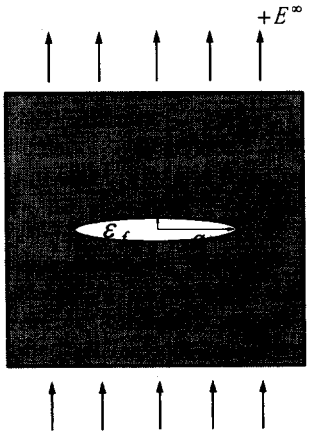


Fig. 1. Schematic illustration of an elliptical flaw in a ferroelectric solid subjected to applied electrical loading.

the Taylor expansion of the right hand side of (4) at $z = a$ and keeping the two leading terms, one obtains

$$-E_1 + iE_2 = iE^\infty\left[\frac{1}{1+\kappa}\frac{\sqrt{a}}{\sqrt{2(z-a)}} + \frac{\kappa}{1+\kappa}\right]. \quad (5)$$

Let the origin of the polar coordinate, $r$ and $\theta$, be located at the right tip of the flaw, as shown in Fig. 1. The electric field outside the flaw is

$$\begin{Bmatrix} E_1 \\ E_1 \end{Bmatrix} = \frac{1}{1+\kappa}\frac{E^\infty\sqrt{\pi a}}{\sqrt{2\pi r}}\begin{Bmatrix} -\sin\dfrac{\theta}{2} \\ \cos\dfrac{\theta}{2} \end{Bmatrix} + \frac{\kappa E^\infty}{1+\kappa}\begin{Bmatrix} 0 \\ 1 \end{Bmatrix}. \quad (6)$$

The first term in (6) represents the singular field governed by the electric intensity factor $K_E = E^\infty\sqrt{\pi a}$, and the second term the uniform electric field. As can be seen from (6), the electric field solution for an impermeable crack is recovered in the vicinity of the flaw for the case of $\kappa \ll 1$. If the aspect ratio $b/a$ is an order of magnitude larger than the ratio of permittivities $\epsilon_f/\epsilon_m$, the impermeable crack solution serves as a good approximation. The region dominated by the first singular term shrinks as $\kappa$ increases. At the other extreme of $\kappa \gg 1$, the uniform electric field prevails in most regions around the crack tip and the conducting crack solution is recovered. If $b/a$ is comparable to $\epsilon_f/\epsilon_m$, electric field effects of both terms should be included.

The stress field near the switching zone boundary may be approximated by the remote $K$ field

$$\sigma_{ij} = \frac{K_{app}}{\sqrt{2\pi r}}\sum_{ij}(\theta), \quad (7)$$

where $K_{app}$ denotes the applied stress intensity factor and $\sigma_{ij}(\theta)$ the universal stress angular distribution.

### 2.2. Switching criterion

An electric field may rotate the polar direction of a domain by either 90 or 180 degrees, but a stress field rotates it only by 90 degrees. A 180° switching does not result in any strain, while a 90° switching results in a fixed strain. Here we adopt the switching criterion proposed by Hwang *et al.* [14] for an individual domain. The criterion states that a domain switches when the electrical work plus the mechanical work exceed a critical value

$$\sigma_{ij}\Delta\epsilon_{ij} + E_i\Delta P_i \geq 2P_sE_c, \quad (8)$$

where $\sigma_{ij}$ is the stress tensor, $\Delta\epsilon_{ij}$ the switching strain tensor, $\Delta P_i$ the polarization switch vector, $E_i$ the electric field vector, $P_s$ the spontaneous polarization and $E_c$ the coercive field. The geometry of the switching zone can be estimated by substituting the stress and electric fields into (8).

## 3. MONO-DOMAIN SOLUTION

We start with the simple case of mono-domain ferroelectrics. The solution obtained in this section will serve as a fundamental solution for the poly-domain ferroelectrics. Consider the plane strain situation. Suppose that all domains are oriented along the poling direction after the polarization process. Global coordinates $X_1$ and $X_2$ are introduced, such that $X_1$ directs along the longer axis of the flaw and $X_2$ normal to it. The uniform initial poling direction forms an angle $\phi$ with the $X_1$ axis.

### 3.1. Geometry of the switching zone

We first estimate the geometry of the switching zone. Consider only 90° switching. There are two possible variants of 90° switching: the domain can switch 90° clockwise or anti-clockwise, with its polarization vector $P_i$ rotating 90° clockwise or anti-clockwise. In global coordinates, the polarization switch vector $\Delta P_i$ can be expressed as

$$\Delta P_i = \sqrt{2}P_s\begin{Bmatrix} \cos\left(\phi \pm \frac{3}{4}\pi\right) \\ \sin\left(\phi \pm \frac{3}{4}\pi\right) \end{Bmatrix}. \quad (9)$$

The values of $-\frac{3}{4}\pi$ and $+\frac{3}{4}\pi$ in (9) correspond to 90° switching clockwise and anti-clockwise, respectively. The switching strain tensor $\Delta\epsilon_{ij}$ is the same for both cases

$$\Delta\epsilon_{ij} = \gamma_s\begin{bmatrix} -\cos 2\phi & \sin 2\phi \\ \sin 2\phi & \cos 2\phi \end{bmatrix}, \quad (10)$$

where $\gamma_s$ denotes the spontaneous strain associated with 90° switching. Please note that the switching strain is uniform in the entire switching zone, while the stress and electric fields are not. Substituting the stress field (7), the electric field (6), the polarization switch vector (9) and the switching strain tensor (10) into the switching criterion (8), one obtains

$$\frac{1}{\sqrt{2\pi r}}\left[K_{app}\gamma_s\sin\theta\sin\left(2\phi + \frac{3}{4}\theta\right) + \frac{\sqrt{2}}{1+\kappa}K_EP_s\sin\left(\phi \pm \frac{3}{4}\pi - \frac{\theta}{2}\right)\right]$$

$$= 2P_sE_c\left[1 - \frac{E^\infty}{\sqrt{2}E_c}\frac{\kappa}{1+\kappa}\sin\left(\phi \pm \frac{3}{4}\pi\right)\right], \quad (11)$$

where $r$ now outlines the boundary of the switched domain from the crack tip. The shape of the switching zone, in terms of a relation between the radius $r$ and the polar angle $\theta$ can be expressed

as follows

$$\sqrt{r} = \sqrt{\rho} R(\theta; \beta, \kappa), \tag{12}$$

where the value

$$\rho = \frac{1}{8\pi}\left(\frac{K_{app}\gamma_s}{P_s E_c}\right)^2 \tag{13}$$

gives a reference scale of the domain switching zone around the crack tip, and the dimensionless parameter

$$\beta = \frac{K_E P_s}{K_{app}\gamma_s} \tag{14}$$

measures the relative magnitude between the non-uniform electric field and the non-uniform stress field. The dimensionless function $R(\theta; \beta, \kappa)$ in (12) can be written explicitly as

$$R(\theta; \beta, \kappa) = \frac{\frac{\sqrt{2}}{1+\kappa}\beta \sin\left(\phi \pm \frac{3}{4}\pi - \frac{\theta}{2}\right) + \sin\theta \sin\left(2\phi + \frac{3}{2}\theta\right)}{1 - \frac{E^\infty}{\sqrt{2}E_c}\frac{\kappa}{1+\kappa}\sin\left(\phi \pm \frac{3}{4}\pi\right)}. \tag{15}$$

As mentioned above, $-\frac{3}{4}\pi$ and $+\frac{3}{4}\pi$ in (15) correspond to clockwise and anti-clockwise 90° switching. The actual switching selects the direction with higher algebraic value of $r$. This can be explained on the physical ground that switching prefers the direction along which reorientation requires less work. Figure 2(a) and (b) exhibit the effects of electric fields on the geometry of the switching zone. The two terms in the numerator of (15) represent the influences from the singular electric field and the stress field, respectively. The effect of the uniform electric field is shown in the denominator of (15). While the singular electric field changes both the shape and the size of the switching zone, the uniform electric field only modifies the size of the switching zone. The relative contribution between the singular electric field and the uniform electric field, namely the first and the second terms in the expansion (6), is measured by the parameter $\kappa$. For the case of $\kappa = 10^3$, uniform electric field dominates, and the switching zone geometry is shown in Fig. 2(a). Since the first term in the numerator of (15) is negligible, the switching zone geometry becomes insensitive to the values of $\beta$. As the applied electric field varies, the size of the switching zone varies, but not its shape. A positive electric field reduces the size of the switching zone, while a negative one enlarges it. For the opposite case of $\kappa = 10^{-3}$, the effect of singular electric field dominates, and the switching zone geometry is shown in Fig. 2(b). Both the shape and the size of the switching zone are changed by varying the remote electric field, and either a positive or a negative electric field enlarges the size of switching zone.

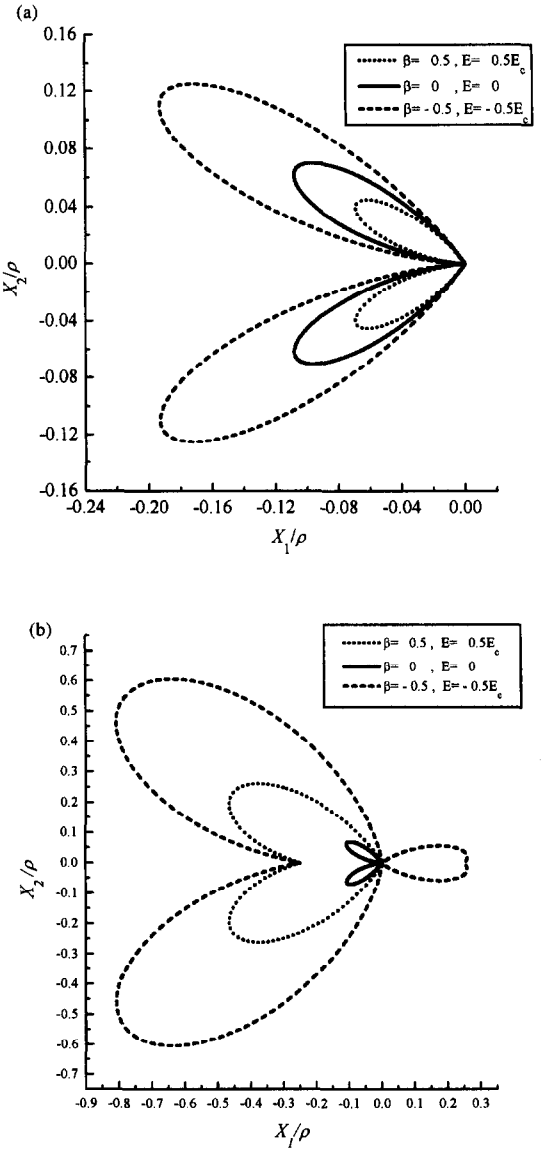


Fig. 2. Domain switching boundary of mono-domain ferroelectrics [$\phi = (\pi/2)$] under positive and negative electric fields. (a) $\kappa = 10^3$; (b) $\kappa = 10^{-3}$.

In formula (12), the positive nature of $\sqrt{r}$ requires that $R(\theta; \beta, \kappa)$ is greater than zero. This condition determines the initial angles, denoted as $\theta_i^+$ and $\theta_i^-$, for polarization switching above and below the crack extension line. The terminating angles, $\theta_f^+$ and $\theta_f^-$, refer to the polar angles where the switching zone above and below the crack reach the maximum heights. These angles can be determined numerically.

### 3.2. *Toughness variation for steady state crack growth*

For dilatant transformation, it was shown by McMeeking and Evans [8] that $K_{app}$ approaches a steady state value after a crack grows more than the height of the transformation zone. In the transform

ation toughening involving both dilatant and shear contributions, rapid approaching to the steady state asymptote is also anticipated, see Lambropoulos [17]. In this work, we only evaluate the steady state fracture toughness ($\Delta a \ll a$), bearing in mind that it serves as an upper bound.

We first derive the change in crack-tip stress intensity, as a result of switch-induced stress redistribution. Denote $K_{tip}$ as the intrinsic fracture toughness that governs the fracture process near the crack tip. For the ceramics in paraelectric phase, there is no switch toughening. Hence, $K_{tip}$ equals $K_{app}$. For the ceramics in ferroelectric phase, we relate $K_{tip}$ to $K_{app}$ by writing

$$K_{tip} = K_{app} + \Delta K. \tag{16}$$

The toughness increment $\Delta K$ can be evaluated by an Eshelby technique, see [8]. The switching strain induces a thin layer of accommodating body forces $T_i$ on the boundary $\Gamma_s$ of the switching zone. For a growing crack, the frontal switching boundary translates as the crack advances, while the wake remains immobile. $\Delta K$ is given by

$$\Delta K = \oint_{\Gamma_s} T_i h_i \, d\Gamma, \tag{17}$$

where $h_i$ is the near-tip weight function,

$$\begin{Bmatrix} h_1 \\ h_2 \end{Bmatrix} = \frac{1}{2(1-\nu)\sqrt{2\pi r}} \times \begin{Bmatrix} \cos\frac{\theta}{2}\left(2\nu - 1 + \sin\frac{\theta}{2}\sin\frac{3\theta}{2}\right) \\ \sin\frac{\theta}{2}\left(2 - 2\nu - \cos\frac{\theta}{2}\cos\frac{3\theta}{2}\right) \end{Bmatrix}. \tag{18}$$

Since switching strain is deviatoric, one has

$$T_i = \frac{Y}{1+\nu}\Delta\epsilon_{ij} n_j, \tag{19}$$

where $Y$ denotes the Young's modulus and $\nu$ the Poisson's ratio. The vector $n_j$ represents the outward normal of $\Gamma_s$. Substituting (18), (19) and the switching zone geometry (12) into (17), one obtains the toughness variation,

$$\Delta K(\phi) = \frac{\eta}{8\pi\alpha(\phi)} K_{app}(\phi)[F(\phi) + \beta D(\phi)], \tag{20}$$

where $K_{app}(\phi)$ corresponds to the applied stress intensity factor to produce a near tip stress intensity of $K_{tip}$ for a mono-domain ferroelectrics of orientation $\phi$, and

$$\eta = \frac{Y\gamma_s^2}{(1-\nu^2)P_s E_c}, \tag{21}$$

$$\alpha(\phi) = 1 - \frac{E^\infty}{\sqrt{2}E_c}\frac{\kappa}{1+\kappa}\sin\left(\phi \pm \frac{3}{4}\pi\right), \tag{22}$$

$$\begin{aligned} F(\phi) = &\left[\sin\theta\sin\left(2\phi + \frac{\theta}{2}\right)\sin\left(2\phi + \frac{3}{2}\theta\right)(\cos\theta + 4\nu - 3)\right]_{\theta_f^-}^{\theta_f^+} \\ &-\Big\{(1-\nu)[\sin(4\phi + 3\theta) - \sin(4\phi + \theta) - \sin 2\theta] \\ &+\frac{1}{4}\sin(4\phi + \theta) + \frac{3}{16}\sin(4\phi + 2\theta) - \frac{1}{4}\sin(4\phi + 3\theta) \\ &-\frac{5}{16}\sin(4\phi + 4\theta) + \frac{1}{16}\sin(4\phi + 6\theta)\frac{1}{2}\sin\theta + \frac{1}{4}\sin 2\theta\Big\}_{\theta_i^+,\theta_f^-}^{\theta_f^+,\theta_i^-}, \end{aligned} \tag{23}$$

$$\begin{aligned} D(\phi) = \frac{\sqrt{2}}{1+\kappa}\Bigg\{&\left[\sin\left(\phi \pm \frac{3}{4}\pi - \frac{\theta}{2}\right)\sin\left(2\phi + \frac{\theta}{2}\right)(\cos\theta + 4\nu - 3)\right]_{\theta_f^-}^{\theta_f^+} \\ &-\left[\frac{1}{2}(4\nu - 3)\cos\left(\pm\frac{3}{4}\pi - \phi - \theta\right) + \frac{3}{8}\cos\left(\pm\frac{3}{4}\pi - \phi - 2\theta\right)\right. \\ &\left.-\frac{1}{16}\cos\left(\pm\frac{3}{4}\pi - \phi - 4\theta\right)\right]_{\theta_i^+\,\theta_f^-}^{\theta_f^+\,\theta_i^-}\Bigg\}. \end{aligned} \tag{24}$$

Table 1. Data used in numerical calculation [14]

| | |
|---|---|
| Spontaneous polarization | $P_s = 0.30$ C/m$^2$ |
| Coercive field | $E = 0.36$ MV/m |
| Young's modulus | $Y = 80$ GPa |
| Poisson's ratio | $\nu = 1/3$ |
| Intrinsic fracture toughness | $K_{tip} = 0.6$ MPa/$\sqrt{m}$ |

The dimensionless group of material parameters $\eta$ emerges as the measure of the ratio between the elastic strain energy and the threshold of switching energy. The dimensionless functions $\alpha(\phi)$, $D(\phi)$ and $F(\phi)$ represent the influences of uniform electric field, singular electric field, and stress field on the near tip $K$ field, respectively.

Substituting (20) into (16), one can write the shielding ratio as follows

$$\frac{K_{app}(\phi)}{K_{tip}} = \frac{1 - \dfrac{\eta}{8\pi\alpha(\phi)} \dfrac{K_E P_s}{K_{tip}\gamma_s} D(\phi)}{1 + \dfrac{\eta}{8\pi\alpha(\phi)} F(\phi)}. \tag{25}$$

To evaluate the shielding ratio, we take a numerical iterative scheme. Under a given electric field, an initial $K_{app}(\phi)/K_{tip}$ is assumed. Then geometric parameters $\theta_i^{\pm}$ and $\theta_f^{\pm}$ are determined numerically, and those data are substituted into (23) and (24) to evaluate $F(\phi)$ and $D(\phi)$. A new shielding ratio is estimated according to (25). The procedure is repeated until it converges. Material parameters used in calculation are listed in Table 1. The length of crack-like flaw 2a is assumed to be 2 mm and spontaneous strain 0.003.

Figure 3 shows the variation of shielding ratio as a function of the initial poling direction under non-uniform positive and negative electric field ($\kappa = 1$). A positive electric field directs along the positive $X_2$ axis, and a negative electric field directs along the negative $X_2$ axis. From Fig. 3, it is seen that toughness variation is symmetric about $\phi = 90°$. As the initial poling direction deviates from 90 degrees, the toughness increases for both positive and negative electric fields and reaches the maximum at 0° and 180°. This is in agreement with experimental observation of anisotropic fracture toughness [2]. For the same initial poling direction, toughening effect of the positive electric field is slightly higher near $\phi = 90°$. As the initial poling direction deviates from 90 degrees, the apparent toughness will increase more under the negative electric field and finally exceed the toughness under the positive electric field. The two curves meet at 0° and 180°.

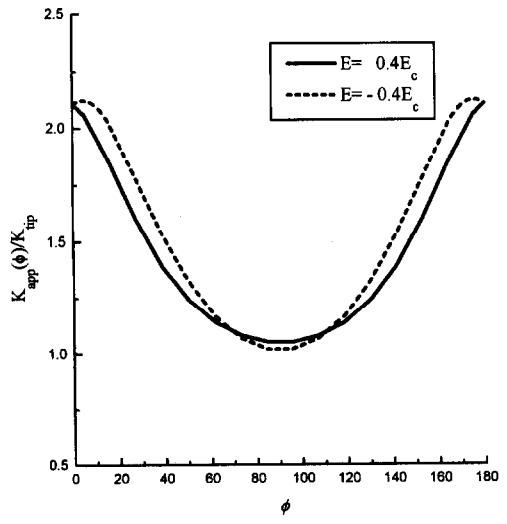


Fig. 3. Effect of positive and negative electric field on the toughness variation of mono-domain ferroelectrics for different initial poling direction $\phi$.

## 4. TOUGHNESS VARIATION FOR FULLY POLED FERROELECTRICS

To estimate toughness variation for poly-domain ferroelectrics, a Reuss type approximation, see Hill [18], is used. Consider a continuum element with poly-domain structure. The orientation distribution function of the domains in that continuum element is denoted by $f(\phi)$. The Reuss approximation assumes that all domains in the continuum element are subjected to the same applied stress and electric fields. Their fates of switching are determined by the switching criterion (8) which relates to their individual orientations. As in all Reuss-type assembly, different switching strains are accommodated without appreciable local interaction. The collective toughening effect is composed of an integration over all orientations (namely with respect to $\phi$) for a specific continuum element, and followed by an area integral for continuum elements in the entire switching zone. For an initially homogeneous ferroelectric aggregate, the domain orientation distributions are the same for all continuum elements. Thus one can switch the order of integrations. The area integral will be carried out first and give rise to the mono-domain solution discussed in the previous section. Further integration with respect to all domain orientations leads to the following superposition integral

$$\Delta K = \int_{-\pi}^{\pi} \Delta K(\phi) f(\phi)\, d\phi. \tag{26}$$

For unpoled ferroelectric ceramics made up of many randomly oriented domains, $f(\phi)$ is uniform for all the directions. Due to the fact that polar axis of a domain can only rotate 90° or 180° from its original direction, it is impossible to align all the domains along the poling direction. For simplicity, we let $f(\phi)$

be uniform for

$$\left[-\frac{\pi}{4}, +\frac{\pi}{4}\right]$$

around the poling direction and vanish elsewhere

$$f(\phi) = \begin{cases} \frac{2}{\pi} & \frac{1}{4}\pi \leqslant \phi \leqslant \frac{3}{4}\pi \\ 0 & \text{otherwise} \end{cases}. \tag{27}$$

Substituting mono-domain solution and the orientation distribution function of domains into (26), one obtains the shielding ratio for fully poled ferroelectrics.

$$\frac{K_{app}}{K_{tip}} = \frac{1 - \frac{\eta}{4\pi^2}\frac{K_E P_s}{K_{tip}\gamma_s}\int_{\frac{\pi}{4}}^{\frac{3\pi}{4}} \frac{D(\phi)}{\alpha(\phi)}\,d\phi}{1 + \frac{\eta}{4\pi^2}\int_{\frac{\pi}{4}}^{\frac{3\pi}{4}} \frac{F(\phi)}{\alpha(\phi)}\,d\phi}. \tag{28}$$

To evaluate the shielding ratio for fully poled ferroelectrics, we take the iterative scheme described in the previous section. Material parameters are listed in Table 1 and spontaneous strain is assumed to be 0.005. To maintain the small scale switching situation, we take the applied electric field from $-0.5E_c$ to $+0.5E_c$. It is instructive to analyze two extreme cases.

*Case 1. Conducting flaw.* In this case, $\kappa \to \infty$, and the electric field is uniform. As studied by Yang and Zhu [7], toughness variation will be gauged by the uniform electric field. In Fig. 4(a) it is seen that shielding ratio decreases monotonically for positive electric field, and increases monotonically for a negative one. A positive electric field promotes crack propagation, while a negative one retards it.

*Case 2. Impermeable flaw.* In this case, $\kappa = 0$. Hence, $\alpha(\phi) = 1$ and the singular electric field dominates. Figure 4(b) depicts the variation of shielding ratio with respect to the dimensionless electric field intensity factor. Under a small electric field, positive or negative, the shielding ratio increases slightly and then reaches a maximum. Further increase of the electric field strength will reduce drastically the shielding ratio, or even embrittle the material. Except the slight raise of the shielding ratio at small applied field, the main effect of the singular electric field is to degrade the fracture toughness of ferroelectric ceramics. This prediction agrees qualitatively with the previous analyses based on the singular electric field, see Yang and Suo [6], and Lynch *et al.* [3].

However, no crack is truly impermeable to electric field, filled as it probably will be by atmosphere or ionized gases. The actual situation of crack tip shielding involves both the singular and the uniform electric fields. As revealed by (28), dimensionless parameter $(K_E P_s)/(K_{tip}\gamma_s)$ measures the relative contribution from the singular electric field, and $E/E_c$

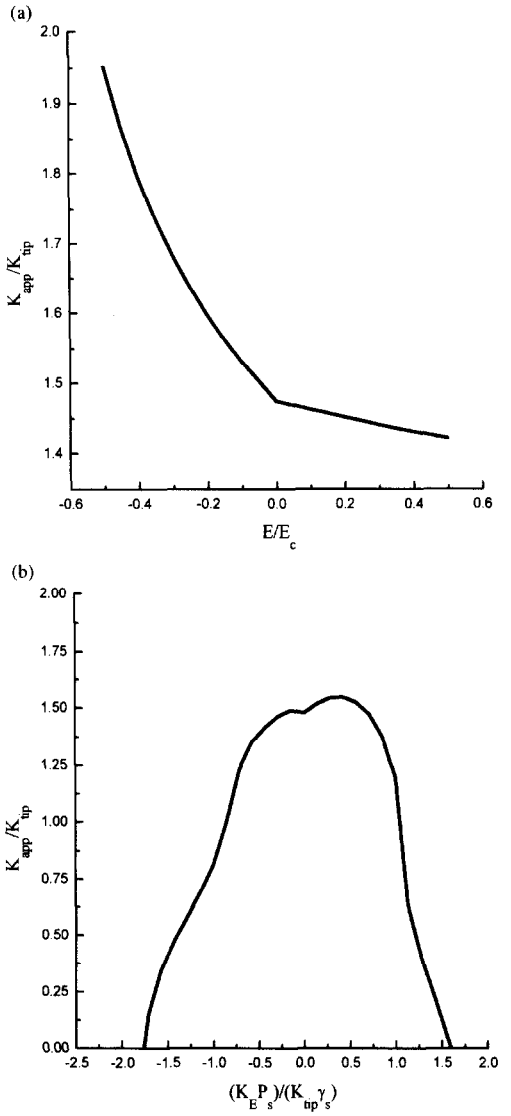


Fig. 4. Toughness variation of fully poled ferroelectrics under (a) uniform electric field; (b) singular electric field.

(hidden in the expression of function $\alpha$) the relative contribution from the uniform electric field. Their effects are controlled by the relative permeability parameter $\kappa$, which is the dimensionless group of geometric and dielectric constants. Figure 5 demonstrates curves of toughness variation vs applied electric field under different values of $\kappa$, where we take a crack length of $2a = 2$ mm and consequently $(K_E P_s)/(K_{tip}\gamma_s) = 0.57$ as $E = 0.5E_c$. The trend of toughness variation under combined electrical and mechanical loadings is dictated by the relative permeability parameter $\kappa$. With decreasing $\kappa$, the effect of the uniform electric field reduces, and the effect of the singular electric field strengthens. As shown in Fig. 5, the extreme case of a conducting crack (in which the toughness variation is controlled by the uniform electric field) is recovered for the case of $\kappa = 10^3$. With decreasing $\kappa$, the effect of singular electric field becomes appreciable. The extreme case

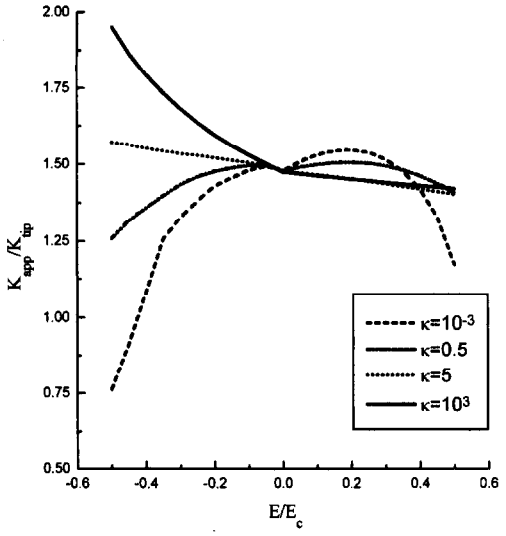


Fig. 5. Shielding ratio as a function of applied electric field under different values of $\kappa$.

of an impermeable crack (in which the toughness variation is dictated by the singular electric field) is recovered for the case of $\kappa = 10^{-3}$.

Conflicting experimental results about the electric field effects on toughness variation can be explained by the above analyses. The geometry of the crack-like flaw and the permittivity of the material inside the crack may significantly change the effect of electric field on toughness. The experimental data of toughness variation under electric field by Park and Sun [10] gives an asymmetric correlation, suggesting that the uniform electric field might play a dominant role near the switching zone boundary. On the other hand, the effect of the singular electric field might present in the experiment of Singh and Wang [12].

## 5. CONCLUDING REMARKS

The present analysis reveals the relevance of polarization switch to the variation of fracture toughness. The effect of switch toughening can be estimated by (28) for fully poled ferroelectrics. The analysis indicates that large singular electric field, positive or negative, usually degrades the fracture toughness of the materials. While the near tip uniform electric field has an asymmetric and monotonic effect on the variation of fracture toughness, toughening under the negative electric field and embrittling under the positive one. With moderate complication in the numerical procedure, this approach can be generated to the cases of ferroelectrics under arbitrary poling.

The key dimensionless material parameters for the toughness modeling are revealed. They are the relative permeability parameter $\kappa$ defined in (3), the relative strength of the singular electric field $\beta$ defined in (14), and the ratio between the elastic strain energy and the polarization switch energy $\eta$, defined in (21).

The effect of the electric field on the fracture toughness, as indicated in Fig. 5, is rather subtle, and sensitive to the modeling of flaw boundary condition. The change of the relative permeability parameter $\kappa$ may alter the trend of toughness variation with the applied electric field. Accordingly, a regulation of the electric boundary condition for the fracture toughness testing is important to get comparable toughness data.

*Acknowledgements*—The authors offer thanks for the support to this research project by the National Natural Foundation of China.

## REFERENCES

1. Pisarenko, G. G., Chushko, V. M. and Kovalev, S. P., *J. Am. Ceram. Soc.*, 1985, **68,** 259.
2. Mehta, K. and Virkar, A. V., *J. Am. Ceram. Soc.*, 1990, **73,** 567.
3. Lynch, C. S., Yang, W., Collier, L., Suo, Z. and McMeeking, R. M., *Ferroelectrics*, 1995, **166,** 11.
4. Lynch, C. S., personal communication, 1995.
5. Suo, Z., *J. Mech. Phys. Solids*, 1993, **41,** 1155.
6. Yang, W. and Suo, Z., *J. Mech. Phys. Solids*, 1994, **42,** 649.
7. Yang, W. and Zhu, T., *J. Mech. Phys. Solids*, in press.
8. McMeeking, R. M. and Evans, A. G., *J. Am. Ceram. Soc.*, 1982, **65,** 242.
9. Budiansky, B., Hutchinson, J. W. and Lambropoulos, J. C., *Int. J. Solids Struct.*, 1983, **19,** 337.
10. Park, S. and Sun, C. T., *J. Am. Ceram. Soc.*, 1995, **78,** 1475.
11. Tobin, A. G. and Pak, Y. E., *Proc. SPIE, Smart Struct. Mater.*, 1993, **1916,** 78.
12. Singh, R. N. and Wang, H., *Adaptive Materials Systems*, ed. G. P. Carman, C. Lynch and N. R. Sottos, Proc. of AMD-vol. 206/MD-vol.58, ASME, 85-95, 1995.
13. Kumar, S. and Singh, R. N., *Acta mater.*, 1996, **44,** 173.
14. Hwang, S. C., Lynch, C. S. and McMeeking, R. M., *Acta Metall. Mater.*, 1995, **43,** 2073.
15. McMeeking, R. M., *J. Appl. Math. Phys.*, 1989, **40,** 615.
16. Dunn, M. L., *Engng Fract. Mech.*, 1994, **48,** 25.
17. Lambropoulos, J. C., *Int. J. Solids Struct.*, 1986, **22,** 1083.
18. Hill, R., *J. Mech. Phys. Solids*, 1963, **11,** 357.